Green Chemistry

RSC Publishing

COMMUNICATION

View Article Online
View Journal | View Issue

Cite this: *Green Chem.*, 2013, **15**, 1133

Received 5th December 2012,
Accepted 22nd February 2013

DOI: 10.1039/c3gc36955b

www.rsc.org/greenchem

Surface dealloyed PtCo nanoparticles supported on carbon nanotube: facile synthesis and promising application for anion exchange membrane direct crude glycerol fuel cell†

Ji Qi,[a] Le Xin,[a] Zhiyong Zhang,[a] Kai Sun,[b] Haiying He,[c] Fang Wang,[a] David Chadderdon,[a] Yang Qiu,[a] Changhai Liang[d] and Wenzhen Li*[a]

Carbon nanotube-supported surface dealloyed PtCo nanoparticles are synthesized as highly active glycerol oxidation catalysts *via* a facile surfactant and thermo free process. The direct crude glycerol anion exchange membrane fuel cell using this nanocomposite as the anode catalyst (0.5 mg_{Pt} cm^{-2}) can achieve a peak power density of 268.5 mW cm^{-2} at 80 °C and ambient pressure.

Due to the rapidly growing global energy needs and the quickly diminishing fossil fuel resources, people are forced to seek renewable, high performance, cost-effective and environmentally beneficial green energy sources.[1] Anion exchange membrane (AEM)-based direct alcohol fuel cells (DAFCs) have recently attracted enormous attention as a potential solution to alleviate the current energy issues.[2] In high pH media, the reaction kinetics of an oxygen reduction reaction (ORR) at the cathode can be greatly improved due to facilitated charge transfer, and therefore non-precious metal catalysts, such as Ag,[3] Fe/Co based catalysts,[4] can be employed. The mild alkaline electrolyte offers a friendly reaction environment that prevents catalysts from severe degradation. The permeability of alcohol is significantly reduced due to electroosmotic drag, and the operation voltage drop resulting from alcohol crossover can be alleviated. However, the sluggish kinetics of anode alcohol oxidation (accordingly high precious metal loading), low alcohol fuel utilization, and high fuel cost remain the main technical obstacles. There is an urgent need to seek renewable cheap fuels and develop highly active anode catalysts using green methods in order to commercialize AEM-based DAFCs as a sustainable, economical and energy-efficient technology.

Crude glycerol has been mass-produced as a byproduct of the currently blooming bio-diesel manufacturing industry.[5] Due to the high cost of its purification, crude glycerol is just treated as waste, disposed by many bio-diesel plants.[6] Therefore, crude glycerol, including a 70–90 wt% pretreated one ($0.74–0.89 gal^{-1}), is very cheap compared to refined alcohol (>$1.3 gal^{-1}, ESI Table S1†). Here, we suggest using crude glycerol as a non-toxic fuel for DAFCs, which will not only lower fuel cost but also achieve higher fuel efficiency than C_{2+} mono-alcohols (such as ethanol, propanol and butanol). This is because crude glycerol can give out more electrons than C_{2+} mono-alcohols from partial oxidation without C–C bond cleavage, which is difficult at relatively low fuel cell operating temperatures (*e.g.* ≤80 °C).[7] As the final products are tartronate and mesoxalate, the theoretical Faradaic efficiency of glycerol oxidation is as high as 57.1% and 71.4%, making glycerol with a high energy density (24.0 MJ L^{-1}) a more meaningful fuel.

Platinum (Pt) has high activity towards electro-oxidation of alcohol, and it has been identified as the best monometallic electro-catalyst to break the C–C bond of C_{2+} alcohols at relatively low temperatures.[8] Therefore, Pt stands out as one of the most desired catalysts to achieve high power density and fuel utilization efficiency. However, Pt is very expensive (>$50 g^{-1}) due to its rare reserves in the earth's crust, and is still more easily contaminated than other precious metals (*e.g.* Pd),[9] although the intermediate poisoning can be alleviated to some extent due to the weak bonding of chemisorbed intermediates in alkaline media.[10] These drawbacks limit its activity and reaction stability. The rational design of Pt-based catalysts with highly active and self-detoxicating sites and superior durability is critical for developing direct alcohol fuel cell technologies.

[a]*Department of Chemical Engineering, Michigan Technological University, Houghton, Michigan, USA. E-mail: wzli@mtu.edu; Fax: +1-906-487-3213; Tel: +1-906-487-2298*
[b]*Department of Materials Science and Engineering, University of Michigan, Ann Arbor, USA*
[c]*Department of Physics, Michigan Technological University, Houghton, Michigan, USA*
[d]*School of Chemical Engineering, Dalian University of Technology, Dalian, Liaoning, China*

†Electronic supplementary information (ESI) available: Detailed experimental and calculation procedures, single cell and half cell supplementary data. See DOI: 10.1039/c3gc36955b

Previous research efforts have been made to develop Pt-based binary and ternary surface dealloyed catalysts, Pt–M (M = Ni,[11] Cr,[11] Co,[12] Cu,[13] Fe,[14]), for an oxygen reduction reaction (ORR) with enhanced mass activity at the PEMFC cathode. However, the *in situ* voltammetric dealloy methods are not practical in real large-scale syntheses,[15] and very little work has been carried out to study the electro-oxidation of alcohols on the promising dealloyed catalysts. In another study, carbon nanotube (CNT)-supported Pt catalysts with good dispersion—a large electrochemically active surface area (ECSA)—have exhibited high specific and mass activities,[16] and showed great potential for use in DAFCs fed with methanol[16] and ethanol.[17]

In this work, surface dealloyed PtCo nanoparticles supported on carbon nanotubes (SD-PtCo/CNT) were prepared *via* an *ex situ* method and used for glycerol oxidation for the first time. The SD-PtCo/CNT catalyst has a PtCo core and a rough Pt-rich shell structure, which offers several advantages. First, the lattice strain of surface dealloyed nanoparticles and the interaction between surface platinum atoms and sub-layer Co atoms will lower the d-band center of the platinum, leading to weakened chemisorption of oxygenated species.[13,18] The rate-determining step (RDS) of alcohol oxidation in alkaline media was accelerated due to the removal of adsorbed intermediates by adsorbed hydroxyl anions.[19] Thus, the Pt poisoning problem is alleviated by enhanced refreshment of active sites. Second, for a single particle with the same size, a dealloyed Pt nanoparticle has higher surface roughness and larger Pt surface area compared to conventional mono-metallic or multi-metallic nanoparticles, thus leading to a higher electrochemically active surface area (ECSA). Third, multi-wall carbon nanotube supports will form three-dimensional network structures,[20] resulting in enhanced mass transfer of alcohol and OH^-. An unprecedented performance of 268.5 mW cm^{-2} was achieved by using the SD-PtCo/CNT anode catalyst with only 0.5 mg_{Pt} cm^{-2} in a membrane electrode assembly (MEA, with a commercial Fe-based cathode) for direct crude glycerol (88 wt%)/O_2 AEMFC operated at 80 °C and ambient pressure.

The schematic synthesis steps of SD-PtCo/CNT are illustrated in Fig. 1. To make the synthesis steps safer and greener, the particle size of nanoparticles was controlled by the concentration of a precursor solution instead of a conventional hazardous surfactant such as oleylamine or oleic acid. Heat treatment was also avoided during the whole process. The surface of the CNTs was grafted with carboxyl groups for anchoring metal particles. Bimetallic PtCo nanoparticles supported on CNTs (PtCo/CNT) were prepared by simultaneously reducing two metal precursors with the strong reducing agent $NaBH_4$ in an ethanol solvent containing well-dispersed CNTs. Co atoms were subsequently removed from the surface of the PtCo/CNT using diluted HCl. SD-PtCo/CNT with 20 wt% Pt loading was finally obtained with randomly distributed Pt and Co atoms inside the metal nanoparticle (see ESI† for the detailed synthesis process).

Fig. 2 shows the transmission electron microscopy (TEM) images, high-angle annular dark-field scanning transmission

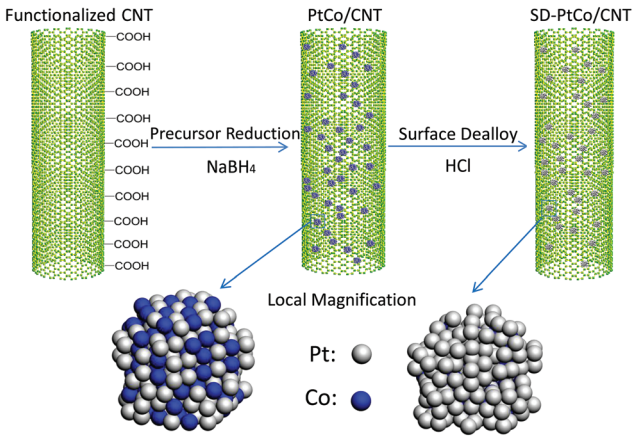

Fig. 1 Schematic illustration of the synthesis of surface dealloyed PtCo supported on CNT (SD-PtCo/CNT) catalyst.

electron microscopy (HAADF-STEM) images of PtCo particles supported on CNTs before and after surface dealloying, and the XRD patterns of Pt/C, Pt/CNT, PtCo/CNT and SD-PtCo/CNT. Fig. 2(A) and (B) indicate that the bimetallic PtCo nanoparticles are well dispersed on CNTs with uniform particle size distribution. The average particle size measured from randomly counting 100 particles was 2.2 nm and 2.3 nm for PtCo/CNT and SD-PtCo/CNT, respectively, which is consistent with the X-ray diffraction (XRD) results calculated using the (220) diffraction peak (see ESI† for calculation details). As marked in Fig. 2(C), the interplanar distance of PtCo/CNT was 0.135 nm and 0.189 nm for facet (220) and facet (200), which is 0.004 nm and 0.008 nm smaller than that of Pt/C, revealing the existence of lattice strain. This was further confirmed by the peak shift of PtCo/CNT compared with Pt/C and Pt/CNT (Fig. 2(E)), which also demonstrates that PtCo is very well alloyed. The characterization results suggest that the presented dealloy technique will not only generate particles with surface roughness (Fig. 2(D)) but also maintain the lattice-strained Pt skeleton structure, since no peak shift is observed for PtCo/CNT and SD-PtCo/CNT (Fig. 2(E)).

Polarization and power density curves of single AEMFC with the SD-PtCo/CNT anode catalyst at different operating temperatures are presented in Fig. 3. Higher temperature improves the glycerol oxidation kinetics, thus leading to a higher fuel cell output power density. The open circuit voltage (OCV) of AEMFC operating at 25 °C, 40 °C, 60 °C and 80 °C was 0.74 V, 0.79 V, 0.80 V and 0.81 V, while the peak power density (PPD) was 35.5 mW cm^{-2}, 52.5 mW cm^{-2}, 91.5 mW cm^{-2} and 141.4 mW cm^{-2} respectively.

Fig. 4 displays polarization and power density curves of a single cell with a Pt/C, Pt/CNT, or SD-PtCo/CNT anode catalyst under optimized conditions (see ESI Fig. S1–S6† for single cell performance under different operating conditions). The OCV of the direct crude glycerol/O_2 AEMFC with SD-PtCo/CNT as the anode catalyst was 0.86 V, which is 0.02 V higher than that with Pt/CNT, 0.07 V higher than that with Pt/C. While the PPD of direct crude glycerol/O_2 AEMFC with SD-PtCo/CNT

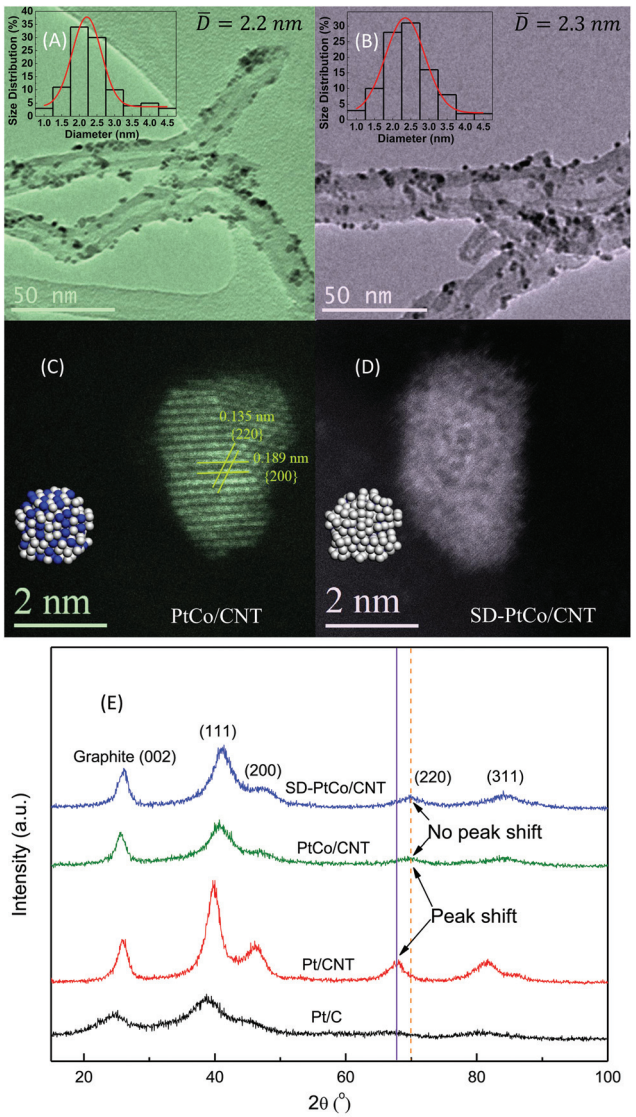

Fig. 2 TEM images and particle size histograms of (A) PtCo/CNT and (B) SD-PtCo/CNT; HAADF-STEM images of a single particle of (C) PtCo/CNT and (D) SD-PtCo/CNT; and (E) XRD patterns of Pt/C (Etek), Pt/CNT, PtCo/CNT and SD-PtCo/CNT (20 wt% Pt loading).

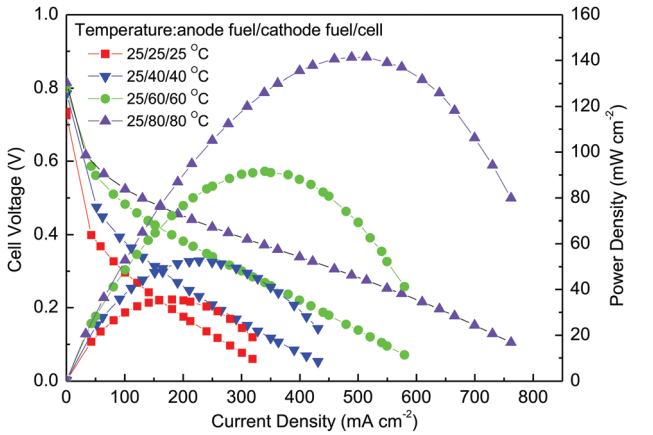

Fig. 3 Polarization and power density curves of direct crude glycerol/O_2 AEMFC with the SD-PtCo/CNT anode catalyst (0.5 mg_{Pt} cm^{-2}) at different temperatures. AEM: Tokuyama A901; cathode catalyst: Fe–Cu–N_4/C (Acta 4020), 3.0 $mg_{catalyst}$ cm^{-2}; anode fuel: 2.0 M KOH + 1.0 M crude glycerol (88 wt%), 1.0 ml min^{-1}; cathode fuel: 100 sccm O_2, ambient pressure.

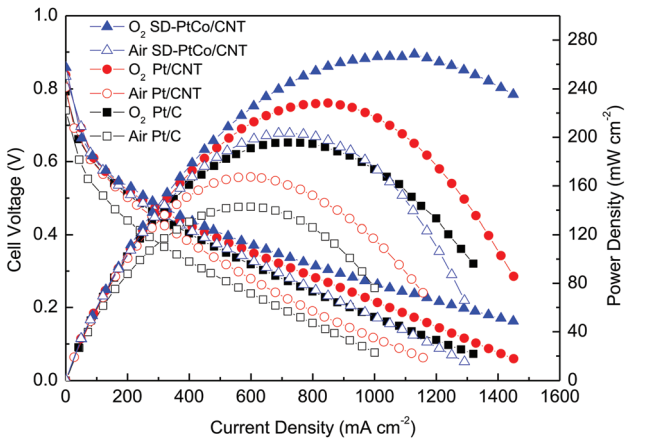

Fig. 4 Polarization and power density curves of direct crude glycerol/O_2 (or air) AEMFC with different anode catalysts (Pt/CNT (Etek), Pt/CNT and SD-PtCo-CNT, 0.5 mg_{Pt} cm^{-2}) under optimized operating conditions. AEM: Tokuyama A901; cathode catalyst: Fe–Cu–N_4/C (Acta 4020), 3.0 $mg_{catalyst}$ cm^{-2}; anode fuel: 6.0 M KOH + 3.0 M crude glycerol (88 wt%), 4.0 ml min^{-1}; cathode fuel: 200 sccm O_2 or 2000 sccm regular air, ambient pressure; temperature (anode fuel–cathode fuel–cell): 25/80/80 °C.

as the anode catalyst was 268.5 mW cm^{-2}, which is 17.6% higher than that with Pt/CNT, and 37.1% higher than that with Pt/C. To the best of our knowledge, the mass activity of 0.537 W $mg_{precious\ metal\ per\ MEA}^{-1}$ based on a single cell at 80 °C is among the highest results published for direct alcohol/O_2 low temperature fuel cells. Moreover, the single cell performance of direct crude glycerol/air AEMFC was about two-thirds of that of direct crude glycerol/O_2 AEMFC. It is also interesting to observe that crude glycerol fuel only resulted in 5.6% AEMFC performance drop compared to high purity glycerol fuel (268.5 mW cm^{-2} *vs.* 284.5 mW cm^{-2}, ESI Fig. S7†).

Electrocatalytic oxidation of high purity glycerol over the three catalysts in half a cell was conducted to clarify their intrinsic activity towards glycerol oxidation. The sequence of mass activity, revealed by the onset potential and peak mass current density in the forward scan, was Pt/C(Etek) < Pt/CNT < SD-PtCo/CNT (ESI Fig. S8†), which is consistent with single AEMFC test results. For Pt/CNT, its large particle size was compensated for by the three-dimensional network catalyst layer,[20] leading to a higher electrochemically active area (ECSA, ESI Fig. S9†) and specific activity (ECSA, ESI Fig. S10†), so that its mass activity remained higher than Pt/C (ESI Fig. S8, S10†). For SD-PtCo/CNT, its ECSA was further enlarged (ESI Fig. S9†) due to smaller particle size and surface roughness, while its specific activity was enhanced by d-band center shift as a result of lattice strain and optimized electronic properties tuned by the sub-layer transitional atoms, so that its mass

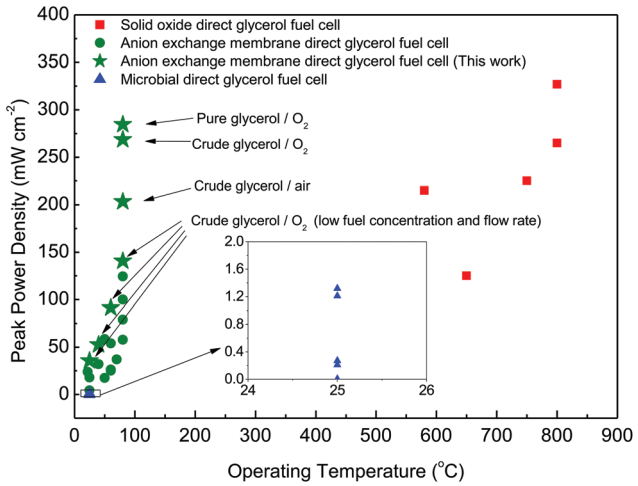

Fig. 5 State-of-the-art glycerol fuel cell performance (see ESI Table S3† for a comparison of experimental details). Peak power density *versus* operating temperature is exhibited for the major glycerol-fed fuel cell systems including the microbial fuel cell (MFC),[22] the anion exchange membrane fuel cell (AEMFC)[7b,c,17,23] and the solid oxide fuel cell (SOFC).[24]

activity is much higher than Pt/CNT and Pt/C (ESI Fig. S8, S10†). The pseudo steady state mass activity after 20 000 s chronoamperometry was 1.5 and 2.4 times that of Pt/CNT and Pt/C, confirming that the long-term activity towards glycerol oxidation has been improved by employing SD-PtCo/CNT (ESI Fig. S11†). The high intrinsic activity of SD-PtCo/CNT towards glycerol oxidation also provided a high fuel utilization ratio in single AEMFC. Compared with Pt/C, SD-PtCo/CNT improved both fuel conversion (by 42.6%–59.2%) and fuel efficiency (by 14.3%–30.8%) at different operating cell voltages (ESI Fig. S12, Table S2†).

Fig. 5 summarizes the state-of-the-art direct glycerol fuel cell performance based on the peak power density and operating temperature. Working at higher temperatures, direct high purity glycerol SOFCs have the highest peak power densities of 225 mW cm^{-2} (580 °C) and 327 mW cm^{-2} (800 °C). This is just slightly higher than the AEMFC performance reported in this work, which is 268.5 mW cm^{-2} (crude glycerol/O_2) and 284.6 mW cm^{-2} (high purity glycerol/O_2). It has been found that OH^- facilitates alcohol oxidation in heterogeneous catalysis.[21] In this work, we demonstrated that facile glycerol oxidation kinetics over dealloyed catalysts in high pH can generate very high electrical power in AEMFC. At 25 °C, 40 °C, 60 °C and 80 °C, the crude glycerol based AEMFC was 97.2%, 64.1%, 69.4% and 78.0% higher peak power density than the maximum published results of high purity glycerol based AEMFC, respectively. In comparison, MFCs work under ambient temperature and pressure, but they only generated a peak power density of <2 mW cm^{-2}, thus limiting its application to environmental remediation rather than practical energy technologies. SOFCs can generate higher electrical power, but they must work at high temperatures (*i.e.* >580 °C), thus limiting them to stationary applications.

Conclusions

We have firstly demonstrated that pretreated crude glycerol (88 wt%) can be directly used as a fuel for high performance AEM-based active DAFCs, which has the potential to substantially impact the development of DAFC technology. CNT-supported surface dealloyed catalysts were employed as AEM-based direct crude glycerol fuel cell anode catalysts, with which an unprecedented single cell performance (268.5 mW cm^{-2}) and catalytic mass activity (537 mW $mg_{\text{precious metal per MEA}}^{-1}$) were achieved under 80 °C and ambient pressure. This performance was found to be comparable with that of SOFC operated under very high temperature (580–800 °C), filling in the gap for low-temperature high-performance direct glycerol fuel cells.

Acknowledgements

We acknowledge the US National Science Foundation (CBET-1159448) for funding and a Michigan Tech REF grant (E49290) for partial support of this work. J. Qi is grateful to the financial support from the Chinese Scholarship Council and L. Xin thanks a Michigan Tech Doctoral Finishing Fellowship.

Notes and references

1 B. W.-L. Jang, R. Gläser, C. Liu and M. Dong, *Energy Environ. Sci.*, 2010, **3**, 253–253.
2 C. Bianchini and P. K. Shen, *Chem. Rev.*, 2009, **109**, 4183–4206.
3 J. S. Spendelow and A. Wieckowski, *Phys. Chem. Chem. Phys.*, 2007, **9**, 2654–2675.
4 (*a*) J. Xu, P. Gao and T. S. Zhao, *Energy Environ. Sci.*, 2012, **5**, 5333–5339; (*b*) L. Xin, Z. Zhang, J. Qi, D. Chadderdon and W. Li, *Appl. Catal., B*, 2012, **125**, 85–94.
5 D. T. Johnson and K. A. Taconi, *Environ. Prog.*, 2007, **26**, 338–348.
6 E. H. Yu, X. Wang, U. Krewer, L. Li and K. Scott, *Energy Environ. Sci.*, 2012, **5**, 5668–5680.
7 (*a*) S. Y. Shen, T. S. Zhao and Q. X. Wu, *Int. J. Hydrogen Energy*, 2012, **37**, 575–582; (*b*) Z. Zhang, L. Xin and W. Li, *Int. J. Hydrogen Energy*, 2012, **37**, 9393–9401; (*c*) Z. Zhang, L. Xin and W. Li, *Appl. Catal. B: Environ.*, 2012, **119–120**, 40–48.
8 L. Ma, D. Chu and R. Chen, *Int. J. Hydrogen Energy*, 2012, **37**, 11185–11194.
9 S. Shen, T. S. Zhao, J. Xu and Y. Li, *Energy Environ. Sci.*, 2011, **4**, 1428–1433.
10 K. Scott and E. Yu, in *Electrocatalysis of Direct Methanol Fuel Cells*, Wiley-VCH Verlag GmbH & Co. KGaA, 2009, pp. 487–525.
11 P. Mani, R. Srivastava and P. Strasser, *J. Power Sources*, 2011, **196**, 666–673.

12 R. Srivastana, P. Mani, N. Hahn and P. Strasser, *Angew. Chem., Int. Ed.*, 2007, **46**, 8988–8991.
13 M. Oezaslan, F. Hasche and P. Strasser, *ECS Trans.*, 2010, **33**, 333–341.
14 J.-l. Shui, C. Chen and J. C. M. Li, *Adv. Funct. Mater.*, 2011, **21**, 3357–3362.
15 M. K. Debe, *Nature*, 2012, **486**, 43–51.
16 W. Li, C. Liang, W. Zhou, J. Qiu, Z. Zhou, G. Sun and Q. Xin, *J. Phys. Chem. B*, 2003, **107**, 6292–6299.
17 V. Bambagioni, C. Bianchini, A. Marchionni, J. Filippi, F. Vizza, J. Teddy, P. Serp and M. Zhiani, *J. Power Sources*, 2009, **190**, 241–251.
18 F. H. B. Lima, J. F. R. de Castro, L. G. R. A. Santos and E. A. Ticianelli, *J. Power Sources*, 2009, **190**, 293–300.
19 Z. X. Liang, T. S. Zhao, J. B. Xu and L. D. Zhu, *Electrochim. Acta*, 2009, **54**, 2203–2208.
20 G. Gao and C. D. Vecitis, *ACS Appl. Mater. Interfaces*, 2012, **4**, 6096–6103.
21 B. N. Zope, D. D. Hibbitts, M. Neurock and R. J. Davis, *Science*, 2010, **330**, 74–78.
22 (*a*) R. L. Arechederra, B. L. Treu and S. D. Minteer, *J. Power Sources*, 2007, **173**, 156–161; (*b*) D. Xing, Y. Zuo, S. Cheng, J. M. Regan and B. E. Logan, *Environ. Sci. Technol.*, 2008, **42**, 4146–4151; (*c*) R. L. Arechederra and S. D. Minteer, *Fuel Cells*, 2009, **9**, 63–69; (*d*) Y. Feng, Q. Yang, X. Wang, Y. Liu, H. Lee and N. Ren, *Bioresour. Technol.*, 2011, **102**, 411–415; (*e*) V. R. Nimje, C.-Y. Chen, C.-C. Chen, H.-R. Chen, M.-J. Tseng, J.-S. Jean and Y.-F. Chang, *Bioresour. Technol.*, 2011, **102**, 2629–2634.
23 (*a*) K. Matsuoka, Y. Iriyama, T. Abe, M. Matsuoka and Z. Ogumi, *J. Power Sources*, 2005, **150**, 27–31; (*b*) S. R. Ragsdale and C. B. Ashfield, *ECS Trans.*, 2008, **16**, 1847–1854; (*c*) V. Bambagioni, M. Bevilacqua, J. Filippi, A. Marchionni, S. Moneti, F. Vizza and C. Bianchini, *Chim. Oggi*, 2010, **28**, VII–X; (*d*) A. Ilie, M. Simoes, S. Baranton, C. Coutanceau and S. Martemianov, *J. Power Sources*, 2011, **196**, 4965–4971.
24 (*a*) J. Y. Won, H. J. Sohn, R. H. Song and S. I. Woo, *ChemSusChem*, 2009, **2**, 1028–1031; (*b*) M. Lo Faro, M. Minutoli, G. Monforte, V. Antonucci and A. S. Aricò, *Biomass Bioenergy*, 2011, **35**, 1075–1084; (*c*) H. Qin, Z. Zhu, Q. Liu, Y. Jing, R. Raza, S. Imran, M. Singh, G. Abbas and B. Zhu, *Energy Environ. Sci.*, 2011, **4**, 1273–1276.